Journal of Power Sources 229 (2013) 190–197

Contents lists available at SciVerse ScienceDirect

Journal of Power Sources

journal homepage: www.elsevier.com/locate/jpowsour

Capacity fading mechanism of $LiFePO_4$-based lithium secondary batteries for stationary energy storage

Jae-Hun Kim, Sang Cheol Woo, Min-Sik Park, Ki Jae Kim, Taeeun Yim, Jeom-Soo Kim*, Young-Jun Kim

Advanced Batteries Research Center, Korea Electronics Technology Institute, Seongnam, Gyeonggi 463-816, Republic of Korea

HIGHLIGHTS

- Capacity fading mechanism of graphite/$LiFePO_4$-based Li-ion batteries is investigated.
- Laminated pouch type 1.5 Ah full cells were cycled 1000–3000 times at a rate of 4C.
- Loss of active lithium by deterioration of graphite electrodes is a primary source for capacity fading.
- Increased electrode resistance in $LiFePO_4$ electrodes is suggested to be the cause of power fading.

ARTICLE INFO

Article history:
Received 5 October 2012
Received in revised form
3 December 2012
Accepted 6 December 2012
Available online 13 December 2012

Keywords:
Lithium ion battery
Lithium iron phosphate
Graphite
Long-term cycling
Capacity fading

ABSTRACT

We report on the capacity fading mechanism of Li-ion batteries consisting of a graphite negative electrode and an olivine $LiFePO_4$ positive electrode during long-term cycling. Laminated pouch type 1.5 Ah full cells are cycled 1000–3000 times at a rate of 4C and the full cells exhibit capacity losses of 10–15%. Half-cell study after full cell disassembly, using degraded electrodes, shows that considerable capacity loss occurs for the negative electrode even at low rates, but the total rate performance of the negative electrode is relatively better than that of the positive electrode. The initial capacity of the positive electrode is largely recovered under low rate conditions (0.1–0.5C), whereas a decline in the reversibility is observed at higher rates (1–5C). Loss of the active lithium source from the system is proposed as a primary source of capacity fading for the full cells. This loss is attributed to a change of the solid electrolyte interface during cycling as well as physical deterioration of the negative electrode due to the intrinsic volume change of the graphite electrode. On the other hand, the increased electrode resistance in the positive electrode is suggested to be the root cause of power fading.

1. Introduction

The ever-increasing global energy, fuelled by the depletion of fossil fuels, has driven the search for renewable energy as a potential alternative energy source. Renewable energy is generally produced using energy conversion systems such as solar cells and wind turbines. Because the energy delivery through energy conversion from renewable sources is unpredictable and intermittent, combination with energy storage systems (ESSs) is required to improve the system efficiency [1]. Rechargeable batteries have been regarded as promising candidates for ESSs, where the Li-ion battery is one of the most commercially verified systems. Practical demonstrations of the feasibility of Li-ion batteries are actively being undertaken worldwide [1,2].

Long-term reliability is requisite for the utilization of Li-ion batteries in ESS. In terms of cycling stability and energy density, graphite remains the first choice among the negative electrode materials [3–5]. $LiFePO_4$ has attracted much attention as a promising positive electrode material because of the low cost, Fe availability, good electrochemical cycling stability, and environmentally friendliness [6,7]. Since the initial report on the electrochemical properties [8] and the subsequent improvement of the low electronic conductivity of the olivine phase [9,10], a number of studies on this material have emerged. At present, the combination of the graphite negative electrode and the $LiFePO_4$ positive electrode for use in Li-ion batteries is one of the most promising cell chemistry for ESS application on the basis of several factors such as cost, energy density, and cycling stability [11–22].

Investigation of the failure mechanism of batteries is of vital importance to the design of durable batteries. Evaluation of the temporal decline in capacity and power fading is difficult given that the degradation of batteries is influenced by various factors and the

* Corresponding author. Tel.: +82 31 789 7491; fax: +82 31 789 7499.
E-mail address: js_energy@keti.re.kr (J.-S. Kim).

0378-7753/$ – see front matter © 2012 Elsevier B.V. All rights reserved.
http://dx.doi.org/10.1016/j.jpowsour.2012.12.024

underlying mechanism is very complicated [23–30]. Conclusive determination of the origin of performance fading may facilitate enhanced design and effective use of these batteries. Although there are reports related to the cell-failure analysis of Li-ion batteries comprising a graphite negative electrode and $LiFePO_4$ positive electrode [12–19], further studies of these systems remain necessary given that the origin of capacity and power fading after accelerated long-term cycling has not been clearly elucidated. Postmortem analysis of the laminated full cells after extensive cycle testing at a high rate can furnish more in-depth understanding and insight into the mechanistics of the graphite/$LiFePO_4$ system, thereby enabling further improvement of the properties of cell components and cell design.

In this study, pouch type 1.5 Ah full cells were assembled by employing commercial-grade graphite and $LiFePO_4$ as electrode materials. The 1.5 Ah cells were designed to mimic the 50 Ah grade cells employed in commercial ESS systems. It was confirmed that the cell-failure modes of both 50 and 1.5 Ah cells were similar in advance. After 1000, 2000, and 3000 cycles at a rate of 4C, each full cell was dismantled and the electrodes were analyzed using various electrochemical and physical analysis tools, and the results are presented herein.

2. Experimental

Commercial-grade graphite and $LiFePO_4$ were, respectively, used as negative and positive electrode materials. The detailed information on the active materials is included in Supplementary data (Fig. S1). Pouch type 1.5 Ah cells were prepared by stacking 12 negative and 11 positive electrodes. Double-side coated electrodes were laminated with polypropylene separators to prevent physical contact and consequent short-circuit. The total capacity (mAh) of the graphite negative electrode was designed to be 1.2 times larger than that of the $LiFePO_4$ positive electrode to prevent Li metal deposition on the negative electrode surface resulting from the lack of negative electrode capacity. Pouch cells were sealed in an aluminum-laminated polymer film bag after the injection of an electrolyte comprising 1 M $LiPF_6$ in ethylene carbonate (EC)/ethyl methyl carbonate (EMC) (3:7 volume ratio) containing 2wt% vinylene carbonate as an additive. All cell fabrication processes were conducted in a dry room with the dew point controlled to less than −50 °C. The full cells were first subjected to a formation cycle by charging and discharging at a very low rate of 0.1C to produce a stable solid electrolyte interface (SEI) layer on the surface of the negative electrode. The cells were then cycled at a rate of 1C. Each full cell was subsequently cycled 1000, 2000, and 3000 times within a voltage range of 2.0–3.8 V at 4C. The high rate of 4C was applied to accelerate the degradation process of the full cells. Following the high-rate cycling, the cells were again cycled 3 times at 1C for evaluation of the level of capacity retention and recovery.

For the analysis of each electrode, the full cells were disassembled in the fully discharged state (see Fig. S2 in the Supplementary data). The negative and positive electrodes were thoroughly washed in pure EMC solutions and dried under vacuum to eliminate the effect of the $LiPF_6$ salt. The electrodes were then analyzed as follows: X-ray diffraction (XRD) was carried out on the electrode using a PANalytical Empyrean XRD system with Pixel^{3D} detector and Cu-Kα radiation (40 kV and 30 mA). The morphology and microstructure of the electrodes were observed by using a field emission scanning electron microscope (FE-SEM, JEOL JSM-7000F) with energy dispersive X-ray spectroscopy (EDS). For SEM observations, cross-sectioned electrodes were prepared using a cross-section polisher (CP, JEOL /sn-09010). Electrochemical impedance spectroscopy (EIS) data were obtained at an amplitude of 10 mV (AC) in the frequency range of 1 MHz to 10 mHz. X-ray photoelectron spectroscopy (XPS, Thermo Scientific Sigma Probe) was used

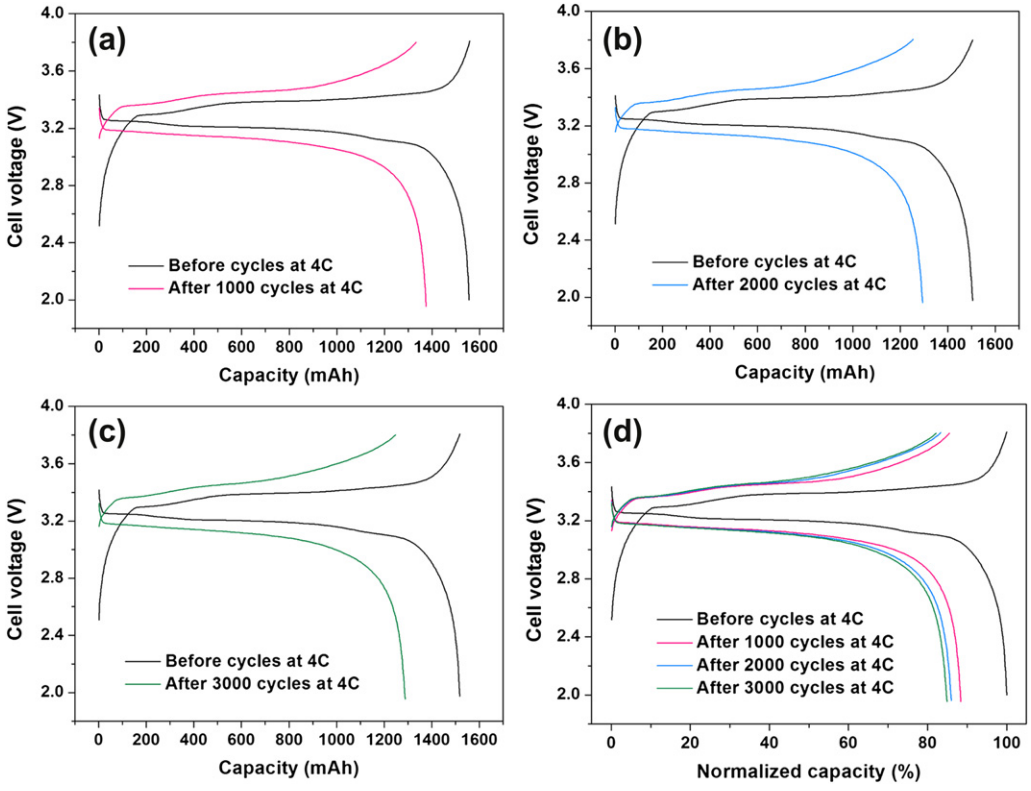

Fig. 1. Voltage profiles at 1C for each full cell before and after (a) 1000, (b) 2000, (c) 3000 cycles at 4C, and (d) comparison of all profiles as normalized capacity.

for determining the composition of the electrode surface. XPS depth analysis was also performed by etching the electrodes with an Ar-ion beam. The half-cell performance of the individual cycled graphite and $LiFePO_4$ electrodes was evaluated in fresh electrolyte by using lithium metal foil as the counter/reference electrode. Fourier-transform infrared spectroscopy (FT-IR, Bruker VERTEX 70) was employed to analyze the chemical composition of the SEI layer. The FT-IR spectra were acquired in the transmission mode at a resolution of 4 cm^{-1}. The electrode samples for spectroscopy analyses were prepared in an Ar-filled glove box in order to avoid reaction with ambient atmosphere. The half-cells were cycled galvanostatically at various current rates using a battery tester (MACCOR Series 4000 system). All analytical and electrochemical experiments were conducted at room temperature.

3. Results and discussion

Fig. 1 shows the voltage profiles of the full cells at 1C (constant current of 1.5 A) before and after different numbers of cycles ranging from 1000 to 3000, at a rate of 4C. The data confirm that at 1C, the reversible capacities of all the pouch cells after cell assembly are close to the designed value of 1.5 Ah. The observed profiles are typical of graphite/$LiFePO_4$ full cells, and the average voltage for discharge was about 3.2 V, which is consistent with previous reports [12]. Following high-rate cycling, increased polarization was observed in the voltage profiles of all the cells, which may be due to increased resistance in the cell components. The cell capacity also declined as a result of cell deterioration during repetitive cycling. The discharge capacities at 1C before and after the long-term cycling are compared in Table 1. The majority of capacity fading occurred during the first 1000 cycles, with a retention rate of 88.4%, whereas the level of reduction over the further 2000 cycles was limited (3.5%). Thus, it is clear that the major degradation of the cell components occurred in the early stage of the cycle test for the full cells. Although capacity retention ratios greater than 80% were achieved for all cells, it is still necessary to determine the origin of the cell capacity fade to further enhance the cycle life of the cells for practical ESS application.

The cell performance fading mechanism was evaluated on the basis of half-cell tests using the coin-type configuration, which were performed after disassembling the fully discharged full cell. The half-cells comprised fresh Li foil as counter electrodes, and retrieved positive and negative electrodes from full cells as working electrodes. The recovered capacity and rate characteristics of the $LiFePO_4$ and graphite electrodes were evaluated using these coin cells. Fig. 2a presents the voltage profiles of the fresh and cycled graphite electrodes against the Li electrode at a rate of 1C. It is found that upon cycling, the discharge capacities (Li extraction) at 1C decrease from 352 mAh g^{-1} for the fresh electrode to 288 mAh g^{-1} for the sample subjected to 3000 cycles, indicating that the capacities were not fully recovered after the cycling process at 4C. The capacities at various discharge rates are shown in Fig. 2b. Over the entire range of C-rate, all the negative electrodes exhibit a similar trend in terms of the rate characteristics, with different values at each rate. The capacity decreases gradually as the current rate increases up to 3C, after which the capacity declines precipitously at 5C; this sudden decline might originate from factors related to the electrode design, such as the thickness and density.

Table 1
Discharge capacities at 1C and capacity retention ratios after cycling at 4C.

Sample	Cell capacity before cycle (mAh)	Cell capacity after cycle (mAh)	Capacity retention after cycle (%)
After 1000 cycles	1555	1375	88.4
After 2000 cycles	1504	1293	86.0
After 3000 cycles	1517	1288	84.9

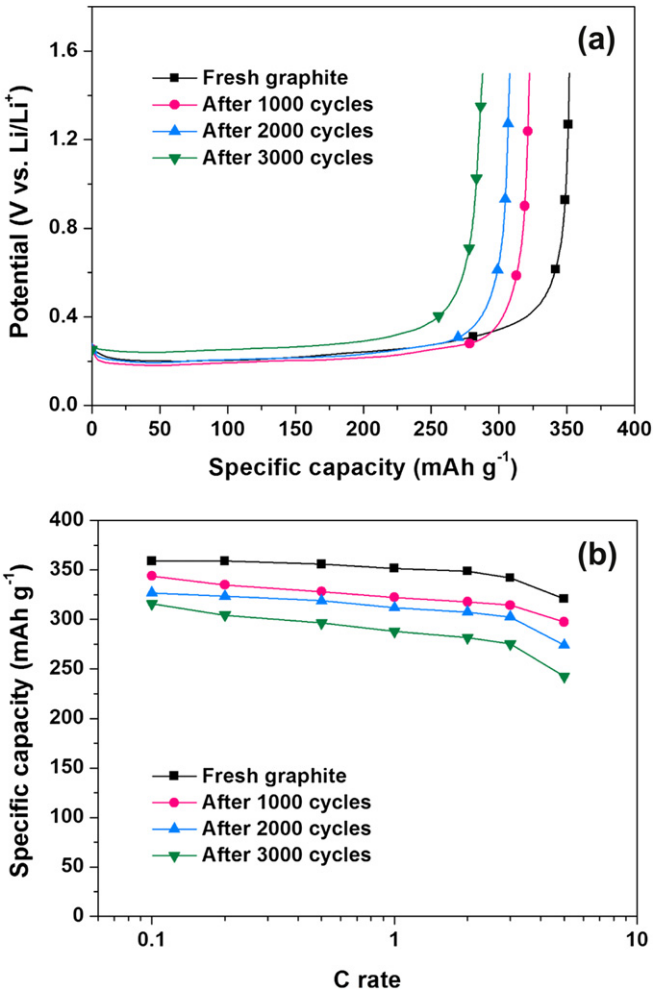

Fig. 2. (a) Voltage profiles of fresh and cycled graphite electrodes at 1C in half-cell and (b) rate characteristics of the electrodes.

XRD patterns and SEM images were acquired for evaluation of the structural and morphological changes of the graphite electrodes during cycling. Only peaks attributable to the graphite phase were observed in the XRD, and secondary phases were not found, indicating that the bulk structure remains intact during cycling, even in the case of 3000 cycles (see Fig. S3 in the Supplementary data). Fig. 3 shows the cross-sectional FE-SEM images of the fresh and cycled electrodes. It can be seen that there are cracks between the graphite particles subsequent to the high-rate cycling process, which indicates the occurrence of physical damage to the graphite electrode due to the intrinsic volume changes that occurred during cycling. There was no notable difference between the cycled electrodes except that the electrode subjected to 3000 cycles exhibited some locally delaminated spots from the Cu current collector.

An electrochemical impedance study was carried out to investigate the interfacial resistance change in the negative electrodes using three-electrode cells in the fully discharged state. The impedance spectra of the electrodes are presented as Nyquist plots in Fig. 4. The spectra are composed of a high-frequency quasi-semicircle and a low-frequency tail. The mid-frequency intercept of the spectra increased with increasing cycling number. The components of the semicircle can generally be assigned to three

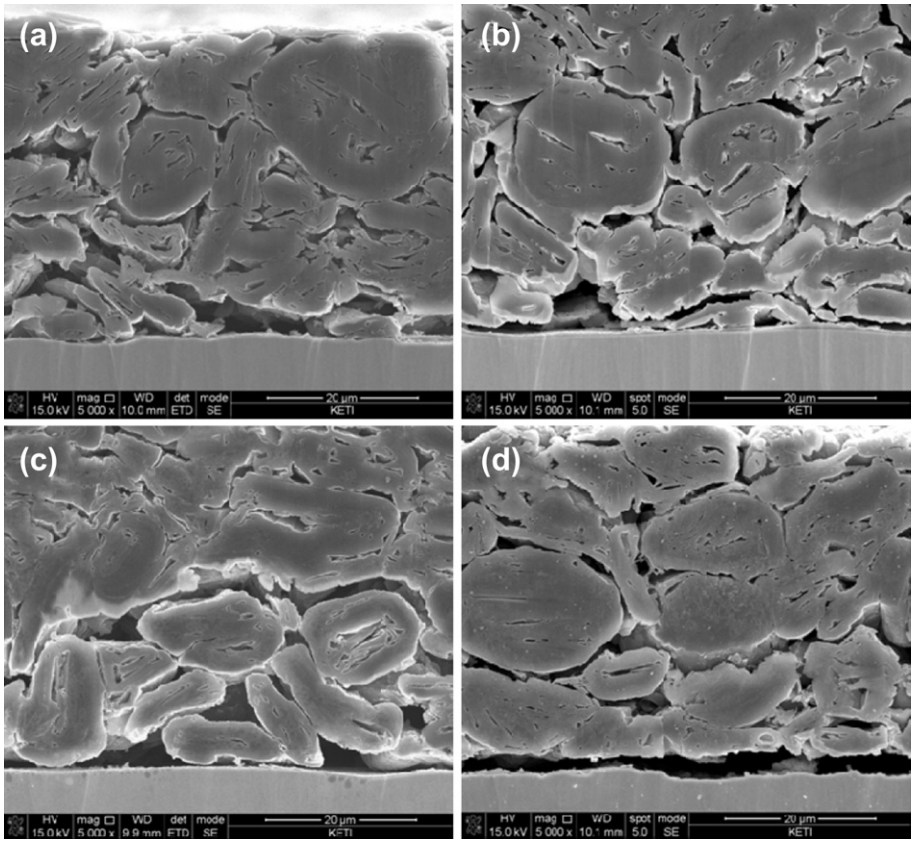

Fig. 3. Cross-sectional FE-SEM images of fresh and cycled graphite electrodes: (a) fresh, after (b) 1000, (c) 2000, and (d) 3000 cycles.

distinctive factors such as the ionic conductivity of the electrolyte, the charge transfer resistance between the active material and the electrolyte, and the double-layer capacitance. These factors correspond to the high-frequency intercept, mid-frequency intercept, and the height of the semicircle, respectively [31–34]. It is inferred from the considerable increase of the mid-frequency intercept (increase in the semicircle diameter) that the interfacial resistance related to the charge transfer between the negative electrode and electrolyte increases significantly upon high-rate cycling. It is well known that SEI film on the graphite surface exerts a significant effect on the electrochemical properties of the active material [35,36]. Reduction of the electrolyte with the Li-ion consumption occurs on the graphite surface during the first Li insertion into the graphite layers. This process leads to the formation of the SEI film, which prevents the negative electrode surface from further reduction of the electrolyte and co-intercalation of the electrolyte components such as solvent molecules [29,35,36]. However, upon the long-term cycling, the SEI film may undergo breakage and reformation resulting from repetitive volume change of the graphite particles, which occurs in response to the movement of lithium ions during cycling. If the rate of lithium intercalation/deintercalation is relatively slow, the volume of the graphite particles also changes slowly resulting in less deformation of the SEI film. In contrast, a rapid movement of lithium ions, as is expected at fast discharge rates such as the rate of 4C used in this study, is expected to result in instability of the SEI film. Under these conditions, breakage of the SEI film is facile and unstable SEI layers are expected to form on the newly exposed graphite surface. This process occurs continuously during the cycle test, thereby inducing increased interfacial resistance, as shown in Fig. 4. In this study, the increased interfacial resistance in the negative electrode can be attributed to the higher resistance of the SEI film resulting from increased thickness or lower ion conductivity of the SEI film [32].

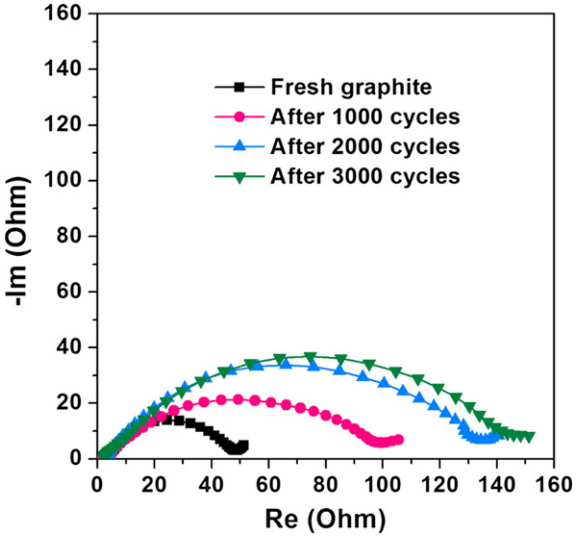

Fig. 4. Electrochemical impedance spectra (Nyquist plot) for fresh and cycled graphite electrodes.

Fig. 5 shows the EDS spectra and corresponding quantitative results obtained from analysis of the surface of the graphite electrodes. Whereas no signal for F and P was found on the fresh electrode, signals attributable to F and P were detected for all the cycled electrodes. The ratios of F and P in the compositions increase

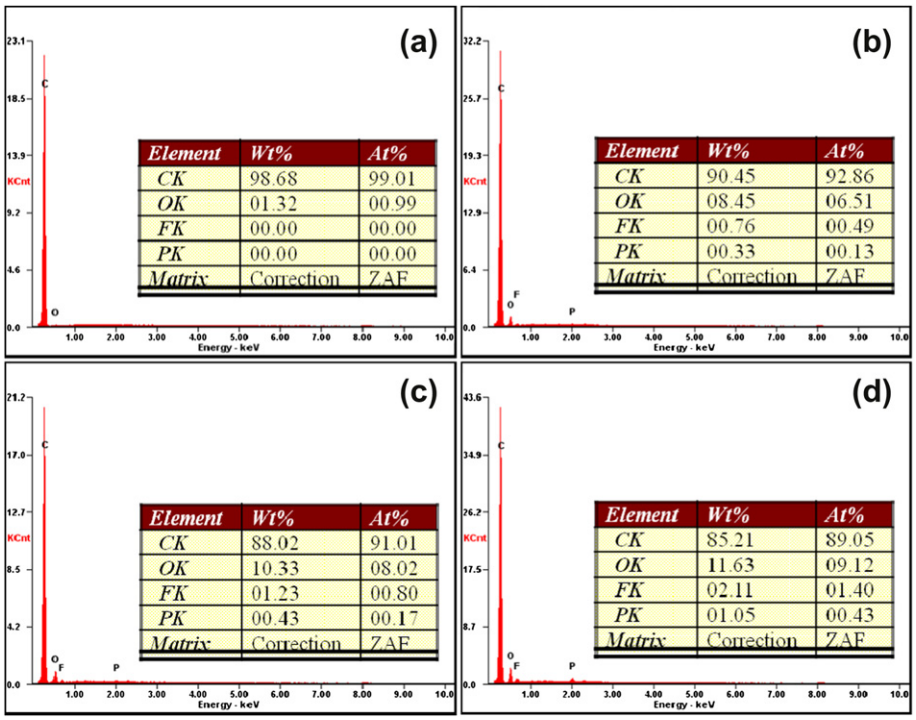

Fig. 5. EDS spectra and quantitative analysis results (inset) of fresh and cycled graphite electrodes: (a) fresh, after (b) 1000, (c) 2000, and (d) 3000 cycles. The electrodes were thoroughly washed with pure EMC solution prior to the measurement.

with increasing number of cycles. The observed signals may indicate the formation of the SEI on the surface of the cycled electrodes since both F and P are major components of the SEI film. When the $LiPF_6$ salt is used in the electrolyte, F and P exist in various forms such as LiF, Li_xPF_y, and Li_xPOF_y [36,37]. Oxygen is another major component of the SEI film and the oxygen content was also found to increase upon cycling. The XPS depth profiles of the cycled graphite electrodes are shown in Fig. 6, which presents the relative atomic ratio of elemental oxygen, fluorine, and phosphorus in the bulk SEI films after cycling. As the cycle number increases, it is clearly observed that the amount of elemental F becomes much higher relative to the other elements. This result suggests that more F was incorporated into the SEI film with increasing cycle number and the major form of the F compounds would be LiF. The presence of LiF on the graphite electrodes was confirmed by means of FT-IR analysis. Peaks assigned to LiF were observed in the regions of ~1500 cm^{-1} and ~870 cm^{-1} and gained intensity with increasing cycle number (see Fig. S4). The observations from the various spectroscopic methods (EDS, XPS, and FT-IR) made herein support the fact that the rise in the interfacial resistance is related to the compositional change of the SEI film. Both the physical deterioration and the increase in the interfacial resistance are ascribed to be the governing factors behind the performance degradation of the graphite electrodes.

Fig. 7 shows the voltage profiles of the fresh and cycled $LiFePO_4$ electrodes at the rate of 1C as well as the discharge capacities at various C-rates measured in a half-cell configuration using Li metal as a counter electrode. Cell polarization, indicated by a voltage drop, increases after 1000 cycles at 4C, whereas no noticeable change is observed as the cycle number is further increased. The $LiFePO_4$ electrodes exhibit a much smaller change in the discharge capacities at 1C (Fig. 7a) relative to the graphite electrodes that exhibited distinctive capacity fading upon cycling (Fig. 2a). The rate characteristics of the cycled $LiFePO_4$ electrodes are evidently different

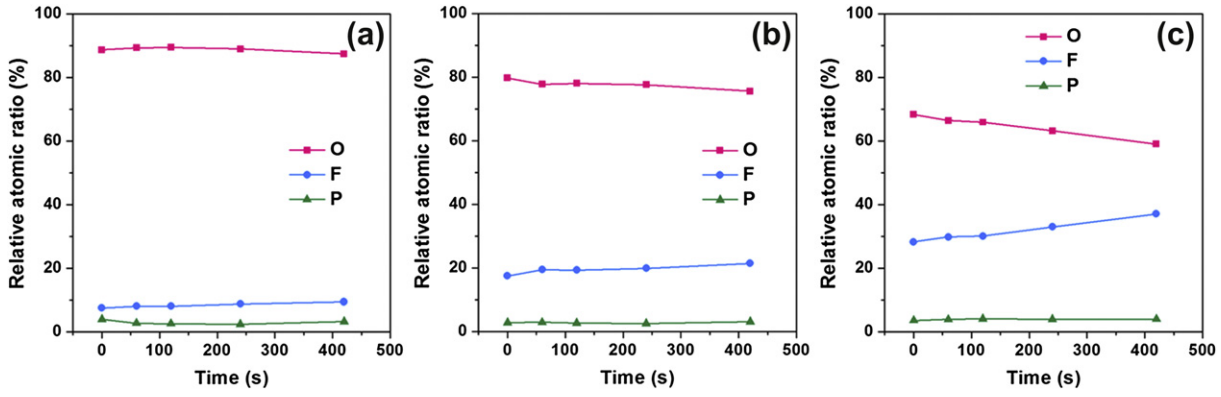

Fig. 6. XPS depth profiles for cycled graphite electrodes: after (a) 1000, (b) 2000, and (c) 3000 cycles. Times in the figures present the Ar-ion sputtering duration.

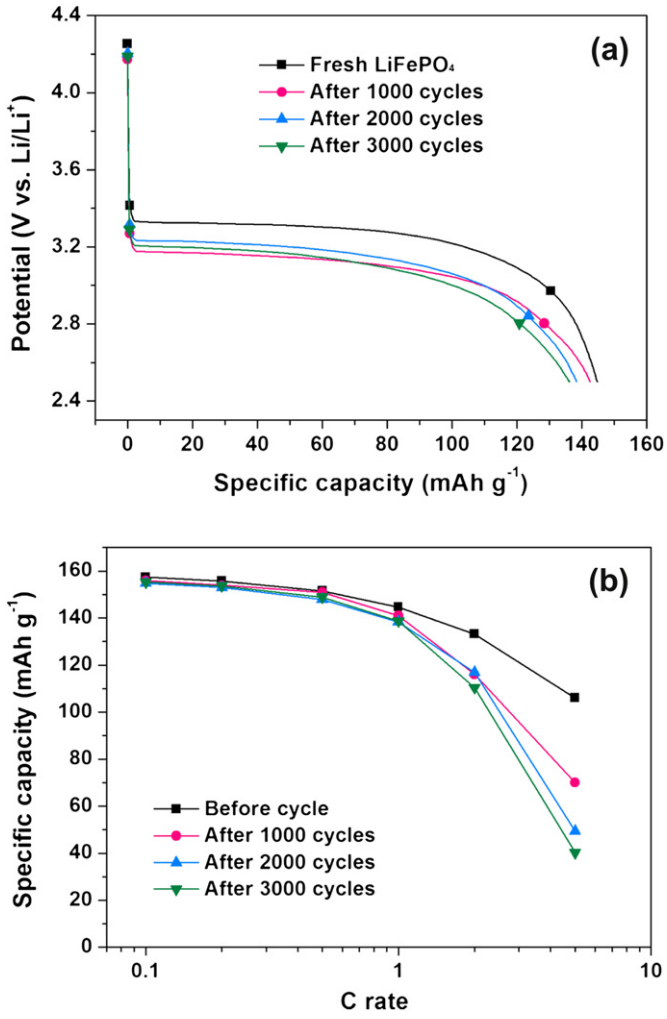

Fig. 7. (a) Voltage profiles of fresh and cycled $LiFePO_4$ electrodes at 1C in half-cell and (b) rate characteristics of the electrode.

from those of the graphite electrodes as shown in Fig. 7b. In the case of the $LiFePO_4$ electrodes, the capacity fading behavior was fairly similar among the electrodes as the rate was varied from 0.1 to 1C. However, considerable capacity loss was observed at the rate of 2C and above. All the cycled electrodes exhibited ca. 86% retention of the capacity of the fresh electrode at 2C, whereas the retention capacity of the electrodes varied with the cycle numbers at 5C. There are distinguishable differences in the rate behavior of the $LiFePO_4$ relative to the graphite electrodes. At low C-rates, the $LiFePO_4$ electrodes exhibited almost the same discharge capacity with increasing cycle number at 0.1C, whereas the graphite electrodes exhibited marked capacity fade under the stated condition. The loss of capacity with increasing current rate was more pronounced for the $LiFePO_4$ electrodes than for the graphite electrode whose fading tendency was maintained up to 5C without abrupt change. This result indicates that performance degradation occurs by different mechanisms for the positive and negative electrodes. Based on the post-electrochemical half-cell analysis, capacity fading of the cycled full cell at low rates could be attributed mainly to failure of the graphite electrode, whereas power fading at high rates was attributed primarily to the $LiFePO_4$ electrode.

Structural and morphological changes in the $LiFePO_4$ electrodes in response to cycling were investigated using SEM and XRD. No remarkable difference in morphology was observed in the cross-sectional SEM images of the fresh and cycled $LiFePO_4$ electrodes (see Fig. S5). Fig. 8 shows the XRD patterns of the fresh and cycled $LiFePO_4$ electrodes in the fully discharged state. $FePO_4$ was detected as a minor phase on all the cycled electrodes. The peak intensity of the $FePO_4$ phase increased gradually with increasing cycle number, and a considerable amount of $FePO_4$ was present in the positive electrode after 3000 cycles. The existence of the $FePO_4$ phase indicates that the active material does not fully participate in the intercalation reaction during discharge. The appearance of the $FePO_4$ phase may be linked either to degradation of the active material or decrease in the available lithium source during cycling. The origin of the $FePO_4$ phase was evaluated using half-cell assemblies comprising the cycled $LiFePO_4$ electrode and fresh Li foil. The half-cells were cycled several times at a low rate of 0.1C prior to disassembly for XRD analysis. In this case, the limitation of the lithium source as a factor would be clearly examined since sufficient lithium ions could be provided to the positive electrode. The XRD results of the positive electrodes retrieved from the half-cells show the absence of the $FePO_4$ phase (Fig. S6), indicating that the appearance of the $FePO_4$ phase does not originate from degradation of active material; rather, it originates from the loss of the active lithium source during the full cell cycling. This result is consistent with the capacity recovery of the positive electrodes at low current rates as shown in Fig. 7a.

Fig. 9 displays the impedance spectra of the fresh and cycled $LiFePO_4$ electrodes. The size of the quasi-semicircles increased upon cycling. The dramatic increase of the mid-frequency intercept values suggests that the interfacial resistance of the electrodes rises as the cycle number increases. When compared to the EIS results of the graphite electrodes, the absolute values of the $LiFePO_4$ electrodes are relatively lower but the increment ratio in the resistance is higher. For electrodes subjected to 1000 cycles, there was an approximately two-fold increase in the interfacial resistance of the graphite electrode relative to the fresh electrode, whereas the $LiFePO_4$ cathode exhibited a four-fold higher resistance than the fresh electrode. This result could be related to the power fading of the full cells and may be attributed to processes at the positive electrode. During rated discharge, the lithium ion moves from the negative electrode to the positive electrode. If the interfacial resistance is increased, then the amount of lithium intercalated into $FePO_4$ is limited by over-potential resulting from the remaining $FePO_4$ phase observed in the XRD patterns. It

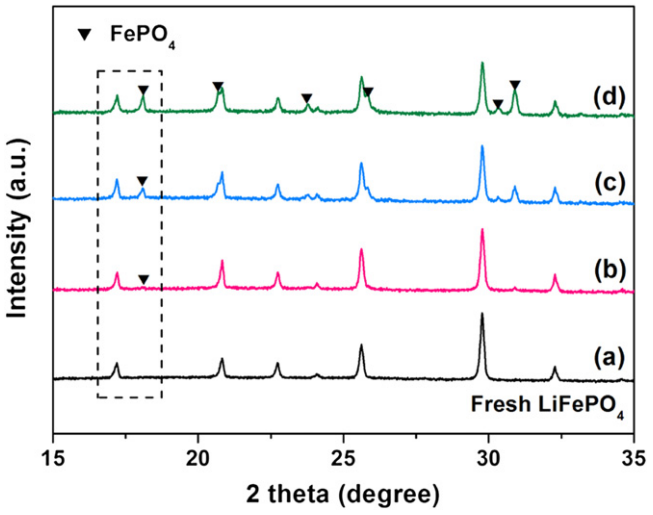

Fig. 8. XRD patterns of fresh and cycled $LiFePO_4$ electrodes: (a) fresh, after (b) 1000, (c) 2000, and (d) 3000 cycles. The full cells were disassembled in the fully discharged state.

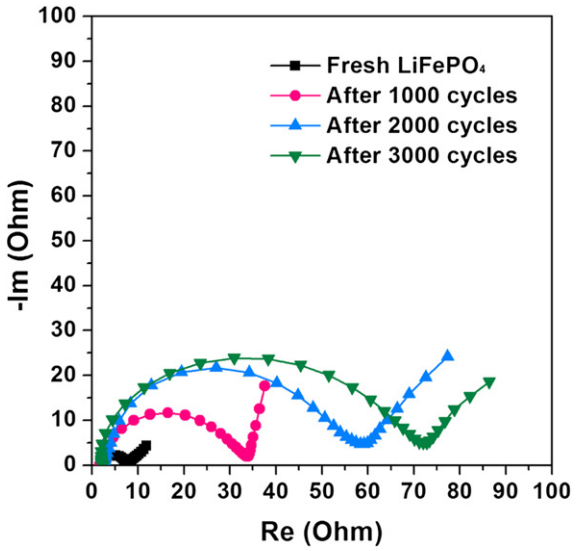

Fig. 9. Electrochemical impedance spectra (Nyquist plot) for fresh and cycled $LiFePO_4$ electrodes. The spectra were measured in the fully discharged state.

appears that the increase in resistance in the positive electrode results in the deterioration of the rate performance as shown in Fig. 7b.

Based on the analyses of both the graphite electrode and $LiFePO_4$ electrode, the mechanism of performance degradation of the full cells upon cycling is discussed as follows. It is clear that the bulk structure of the $LiFePO_4$ electrode remains intact affecting lithium intercalation after extensive cycling. In the case of the graphite electrode, the total capacity was designed to be 1.2 times higher than that of the $LiFePO_4$ electrode in this study. It is believed that the sufficient active sites for Li intercalation remain in the graphite electrode after long-term cycling, even though there was evidence of some physical deterioration in the SEM images. Therefore, the degradation of the active material is not the root cause of capacity fading during long-term cycling for either electrode. It is postulated for the main cause of capacity fading is the loss of active lithium, which was evidenced by the appearance of the $FePO_4$ phase in the XRD patterns of the positive electrodes. This can be explained in view of the fact that SEI formation consumes the active lithium provided by the positive electrode initially. During subsequent cycles, the SEI breaking/repairing process also spends active lithium in the graphite electrode. The active lithium could also be eliminated by physical delamination of the graphite particles from the current collectors. Consequently, the key contributor to capacity fading in the full cells at a relatively low rate (1C) is proposed to be the degradation of the graphite electrode, which is attributed to the intrinsic volume change occurring during cycling. This degradation apparently occurs primarily during the first 1000 cycles, as shown in Table 1 and Fig. 3. On the other hand, a drastic increase of in the interfacial resistance is exhibited by the $LiFePO_4$ electrode, which results in the fading of the rate performance. Therefore, the power fade of full cells may be ascribed to the increasing interfacial resistance of the positive electrode.

4. Conclusions

Laminated pouch type 1.5 Ah full cells were cycled 1000–3000 times at a rate of 4C; the full cells exhibited a capacity loss of 10–15%. Investigation of the capacity fading mechanism by analysis of both graphite and $LiFePO_4$ electrodes retrieved from full cells in the fully discharged states, using various analyses, after 1000, 2000, and 3000 cycles showed that the negative electrode exhibited considerable capacity loss even at low rates, whereas the rate performance was relatively better than that of the positive electrode. Based on electrochemical and structural analyses, capacity fading was attributed to the loss of active lithium by irreversible consumption during the SEI formation/repairing process on the graphite surface and the physical degradation of the graphite electrode due to intrinsic volume changes during cycling. Half-cell tests of the positive electrode demonstrated that most of the capacity was recovered at low rates. However, the reversible capacities at high rates declined dramatically compared to the fresh electrodes due to increased interfacial resistance. The rising interfacial resistance of the positive electrodes may be a contributing factor to the power fading of the full cells.

Acknowledgments

This work was supported by the Energy Efficiency & Resources of the Korea Institute of Energy Technology Evaluation and Planning (20102010100090) grant funded by the Korea Government Ministry of Knowledge Economy.

Appendix A. Supplementary data

Supplementary data related to this article can be found at doi:10.1016/j.jpowsour.2012.12.024.

References

[1] B. Dunn, H. Kamath, J.-M. Tarascon, Science 334 (2011) 928.
[2] Q. Hao, Z. Jianhui, L. Jih-Sheng, Y. Wensong, IEEE Trans. Power Electr. 26 (2011) 886.
[3] S. Flandrois, B. Simon, Carbon 37 (1999) 165.
[4] M. Endo, C. Kim, K. Nishimura, T. Fujino, K. Miyashita, Carbon 38 (2000) 183.
[5] B. Scrosati, J. Garche, J. Power Sources 195 (2010) 2419.
[6] B.L. Ellis, K.T. Lee, L.F. Nazar, Chem. Mater. 22 (2010) 691.
[7] M.S. Whittingham, Chem. Rev. 104 (2004) 4271.
[8] A.K. Padhi, K.S. Nanjundaswamy, J.B. Goodenough, J. Electrochem. Soc. 144 (1997) 1188.
[9] S.-Y. Chung, J.T. Bloking, Y.-M. Chiang, Nat. Mater. 1 (2002) 123.
[10] P.P. Prosini, D. Zane, M. Pasquali, Electrochim. Acta 46 (2001) 3517.
[11] K. Striebel, A. Guerfi, J. Shim, M. Armand, M. Gauthier, K. Zaghib, J. Power Sources 119–121 (2003) 951.
[12] J. Shim, K.A. Striebel, J. Power Sources 119–121 (2003) 955.
[13] K. Zaghib, K. Striebel, A. Guerfi, J. Shim, M. Armand, M. Gauthier, Electrochim. Acta 50 (2004) 263.
[14] K. Striebel, J. Shim, A. Sierra, H. Yang, X. Song, R. Kostecki, K. McCarthy, J. Power Sources 146 (2005) 33.
[15] M. Dubarry, B.Y. Liaw, J. Power Sources 194 (2009) 541.
[16] P. Liu, J. Wang, J. Hicks-Garner, E. Sherman, S. Soukiazian, M. Verbrugge, H. Tataria, J. Musser, P. Finamore, J. Electrochem. Soc. 157 (2010) A499.
[17] K. Amine, J. Liu, I. Belharouak, Electrochem. Commun. 7 (2005) 669.
[18] M. Safari, C. Delacourt, J. Electrochem. Soc. 158 (2011) A1123.
[19] L. Castro, R. Dedryvere, J.-B. Ledeuil, J. Breger, C. Tessier, D. Gonbeau, J. Electrochem. Soc. 159 (2012) A357.
[20] H.-C. Wu, C.-Y. Su, D.-T. Shieh, M.-H. Yang, N.-L. Wu, Electrochem. Solid-State Lett. 9 (2006) A537.
[21] Y. Zhang, C.-Y. Wang, X. Tang, J. Power Sources 196 (2011) 1513.
[22] J. Wang, P. Liu, J. Hicks-Garner, E. Sherman, S. Soukiazian, M. Verbrugge, H. Tataria, J. Musser, P. Finamore, J. Power Sources 196 (2011) 3942.
[23] M. Wohlfahrt-Mehrens, C. Vogler, J. Garche, J. Power Sources 127 (2004) 58.
[24] K. Amine, C.H. Chen, J. Liu, M. Hammond, A. Jansen, D. Dees, I. Bloom, D. Vissers, G. Henriksen, J. Power Sources 97–98 (2001) 684.
[25] X. Zhang, J.P.N. Ross, R. Kostecki, F. Kong, S. Sloop, J.B. Kerr, K. Striebel, E.J. Cairns, F. McLarnon, J. Electrochem. Soc. 148 (2001) A463.
[26] K.A. Striebel, J. Shim, E.J. Cairns, R. Kostecki, Y.-J. Lee, J. Reimer, T.J. Richardson, P.N. Ross, X. Song, G.V. Zhuang, J. Electrochem. Soc. 151 (2004) A857.
[27] J. Shim, R. Kostecki, T. Richardson, X. Song, K.A. Striebel, J. Power Sources 112 (2002) 222.
[28] D.P. Abraham, J. Liu, C.H. Chen, Y.E. Hyung, M. Stoll, N. Elsen, S. MacLaren, R. Twesten, R. Haasch, E. Sammann, I. Petrov, K. Amine, G. Henriksen, J. Power Sources 119–121 (2003) 511.
[29] J. Vetter, P. Novák, M.R. Wagner, C. Veit, K.C. Möller, J.O. Besenhard, M. Winter, M. Wohlfahrt-Mehrens, C. Vogler, A. Hammouche, J. Power Sources 147 (2005) 269.

[30] M. Broussely, S. Herreyre, P. Biensan, P. Kasztejna, K. Nechev, R.J. Staniewicz, J. Power Sources 97–98 (2001) 13.
[31] J. Jamnik, Solid State Ionics 157 (2003) 19.
[32] L.J. Hardwick, M. Marcinek, L. Beer, J.B. Kerr, R. Kostecki, J. Electrochem. Soc. 155 (2008) A442.
[33] P.P. Prosini, M. Lisi, D. Zane, M. Pasquali, Solid State Ionics 148 (2002) 45.
[34] M. Koltypin, D. Aurbach, L. Nazar, B. Ellis, Electrochem. Solid-State Lett. 10 (2007) A40.
[35] D. Aurbach, B. Markovsky, I. Weissman, E. Levi, Y. Ein-Eli, Electrochim. Acta 45 (1999) 67.
[36] D. Aurbach, E. Zinigrad, Y. Cohen, H. Teller, Solid State Ionics 148 (2002) 405.
[37] A.M. Andersson, K. Edstrom, J. Electrochem. Soc. 148 (2001) A1100.